



1 **Using satellite measurements and mesoscale modelling to**
2 **understand the contribution to an extreme air pollution**
3 **event in India**

4
5 Ashique Vellalassery¹, Dhanyalekshmi Pillai, ^{1,*}, Julia Marshall ^{2,#}, Christoph Gerbig², Michael
6 Buchwitz³, and Oliver Schneising³.

7
8
9 ¹ Indian Institute of Science Education and Research Bhopal (IISERB), Bhopal, India

10 * also at Max Planck Partner Group (IISERB) affiliated with the Max Planck Society Munich,
11 Germany

12 ² Max Planck Institute for Biogeochemistry, Jena, Germany

13 [#] now at Deutsches Zentrum für Luft- und Raumfahrt, Institut für Physik der Atmosphäre,
14 Oberpfaffenhofen, Germany

15 ³ Institute of Environmental Physics (IUP), University of Bremen, Bremen, Germany

16

17 *Correspondence to:* Dhanyalekshmi Pillai (dhanya@iiserb.ac.in, kdhanya@bgc-jena.mpg.de)

18



1 **Abstract**

2 Several ambient air quality records corroborate severe and persistent degradation of air quality
3 over North India during the winter months with evidence of a continued increasing trend of
4 pollution across the Indo-Gangetic Plain (IGP) over the past decade. A combination of
5 atmospheric dynamics and uncertain emissions, including the post-monsoon agricultural
6 stubble burning, make it challenging to resolve the role of each individual factor. Here we
7 demonstrate the potential use of an atmospheric transport model, the Weather Research and
8 Forecasting model coupled with chemistry (WRF-Chem) to identify and quantify the role of
9 transport mechanisms and emissions on the occurrence of the pollution events. The
10 investigation is based on the use of CO observations from Tropospheric Monitoring
11 Instrument (TROPOMI), onboard the Sentinel 5-Precursor satellite, and the surface
12 measurement network as well as WRF-Chem simulations to investigate the factors contributing
13 to CO enhancement over India during November 2018. We show that the simulated column-
14 averaged dry air mole fraction (XCO) is largely consistent with TROPOMI observations with a
15 spatial correlation coefficient of 0.87. The surface-level CO concentrations show larger
16 sensitivities to boundary layer dynamics, wind speed, and diverging source regions, leading to
17 a complex concentration pattern and reducing the observation-model agreement with a
18 correlation coefficient ranging from 0.41 to 0.60 for measurement locations across the IGP. We
19 find that daily satellite observations can provide a first-order inference of the CO transport
20 pathways during the enhanced burning period, and this transport pattern is reproduced well in
21 the model. By using the observations and employing the model at a comparable resolution, we
22 confirm the significant role of atmospheric dynamics as well as residential, industrial and
23 commercial emissions in the production of the exorbitant level of air pollutants in North India.
24 We find that biomass burning plays only a minimal role in both column and surface
25 enhancements of CO, except for in the state of Punjab during the high pollution episodes.
26 While the model reproduces observations reasonably well, a better understanding of the factors
27 controlling the model uncertainties is essential to relate the observed concentrations to the
28 underlying emissions. Overall, our study emphasizes the importance of undertaking rigorous
29 policy measures, mainly focusing on reducing residential, commercial and industrial emissions
30 in addition to actions already underway in the agricultural sectors.

31
32
33



1 1. Introduction

2 Biomass burning (BB) has been recognized as the second-largest source of radiatively and
3 chemically active trace gases (e.g. CO, CO₂, and SO₂) and aerosols (e.g. PM₁₀, and PM_{2.5}) in
4 the global atmosphere, which has significant implications for climatic change and human
5 health (Andreae, 2001; Bond, 2004; Crutzen and Andreae, 1990; Guenther et al., 2006; Kaiser
6 et al., 2012; van der Werf et al., 2017). According to previous reports, BB alone accounts for
7 59% of Black Carbon (BC) emissions, one-third to one-half of global carbon monoxide (CO)
8 and 20% of nitrogen oxide (NO_x) emissions (Akagi et al., 2011; Andreae and Jolla, 2019).
9 Based on the model estimates of Ward et al., (2012), in the absence of fire-related emissions,
10 there would be a reduction of about 40 ppm CO₂ from the current atmospheric concentration
11 level, indicating the importance of fire activities for the global carbon budget.

12 In India, emissions from open-biomass burning include significant contributions from
13 agricultural crop residue burning in addition to forest and grassland fires and play an essential
14 role in terms of releasing total carbon content to the atmosphere. Agricultural stubble burning
15 during the post-harvesting period is one of the main kinds of biomass burning practices used in
16 India to clear the land to make it suitable for the next crop (Tai-Yi, 2012; Zha et al., 2013).
17 According to previous estimates, crop waste open burning, which includes its use in residential
18 heating and cooking, is responsible for 78-83% (116–289 Tg yr⁻¹) of the total biomass burned
19 in India during the year 2001 while rest of the contributions are from forest fires
20 (Venkataraman et al., 2006). As per the previous studies, the primary crop residues generated
21 in India are rice straw (112 Mt), wheat straw (109.9 Mt), rice husk (22.4 Mt), sugarcane tops
22 (97.8 Mt) and bagasse (101.3 Mt), the major part of which is burnt in the open air (Lasko and
23 Vadrevu, 2018). Most of these burning activities are found over the northern part of India along
24 the foothills of the Himalayas known as the Indo-Gangetic Plains (hereafter called the
25 IGP). The IGP is a highly populated and very important agro-eco-region in South-Asia, which
26 includes the states of Punjab, Haryana, Bihar, Uttar Pradesh and West Bengal. The region
27 occupies nearly 20% of the total geographical area of India and contributes about 42% to
28 India's total food grains production (Tripathi et al., 2007). Based on VIIRS (Visible Infrared
29 Imaging Radiometer Suite) thermal anomalies, a recent study has estimated burnt crop residues
30 of 20.4 Mt and 9.6 Mt in Punjab and Haryana for the agricultural year 2017-18 in which most
31 of the residue burnt (>90%) at the field was from rice and wheat crops (Singh et al., 2020).

32 Episodes of pollution events are a major concern in the IGP region, which worsen during post-
33 monsoon and winter seasons (Cusworth et al., 2018; Dekker et al., 2019; Girach and Nair,
34 2014). According to the World Air Quality Report 2019 based on ambient PM_{2.5}
35 concentration, fourteen of the top twenty most polluted cities in the world are located in the
36 IGP region, which also includes India's capital region, Delhi. Earlier studies and reports
37 attributed this to several reasons, mainly crop residue burning over Punjab and Haryana, the
38 two adjoining states of India's capital city Delhi (Girach and Nair, 2014; Gupta et al., 2004;
39 Sidhu et al., 1998). However, the contributions from different source sectors and source regions
40 on Delhi's pollution levels still remain highly uncertain, which hinders the implementation of
41 definitive measures to address pollution events. A recent study reported a general lack of
42 reliable data and research efforts on biomass burning related issues on environment and human



1 health (Yadav et al., 2018). Since agricultural stubble burning is a practice prohibited by law in
2 India, official surveys conducted to estimate the extent of fire emission are not reliable. There
3 is, therefore, a critical need to improve the current knowledge base to help to make future
4 policies and implement mitigation strategies.

5 Kaiser et al., (2012) demonstrated an approach for calculating biomass-burning emissions by
6 assimilating satellite-based fire radiative power (FRP) observations in which the combustion
7 rate and trace gas emissions are subsequently derived with land/cover-specific conversion
8 factors and emission factors compiled through literature surveys. While the FRP-based
9 approach has clear advantage in enhancing accuracy compared to other inventory-based
10 datasets such as the Global Fire Emission Database (GFED), several studies have indicated
11 inaccuracies in the derived biomass burning products due to instrument limitations and usage
12 of conversion factors (Cusworth et al., 2018; Dekker et al., 2019; Huijnen et al., 2016; Kaiser
13 et al., 2012; Mota and Wooster, 2018). The recent availability of greenhouse gas satellite
14 observations with unprecedented data density at high spatial and temporal resolution paves the
15 more direct way for a detailed study on the origin, distribution and extent of trace gas levels
16 over a vast domain on a monthly to daily basis. Carbon monoxide (CO) is one of the major
17 gases emitted from biomass burning and incomplete fossil fuel combustion. The major sink of
18 CO is reaction with the hydroxyl radical (OH) to form CO₂ and precursor tropospheric ozone.
19 The lifetime of CO in the atmosphere is between several weeks and several months and varies
20 with the location and season depending on the oxidizing capacity of the environment (Jaffe,
21 1968). Compared to CO₂ and CH₄, the short lifetime of CO makes it easier to detect from the
22 background concentration level and thus it can be a good tracer of pollution transport (Dekker
23 et al., 2017). Therefore, CO can be used as a proxy for the anthropogenic emissions of other
24 pollutants, for example, emissions of important GHGs such as carbon dioxide (Gamnitzer et
25 al., 2006).

26 The TROPospheric Monitoring Instrument (TROPOMI), onboard the Sentinel 5-Precursor
27 satellite, has been measuring various trace gases, including CO since November 2017
28 (Landgraf et al., 2016; Borsdorff et al., 2018a, 2019b; Schneising et al., 2019, 2020).
29 TROPOMI measures with high spatial (7 km × 7 km) and temporal resolution (global daily
30 coverage, not accounting for cloud and aerosol contamination). The unprecedented data
31 density, with high spatial and temporal resolution, makes TROPOMI useful for getting
32 information from city-scale to large-scale. The validation of the TROPOMI retrieval with
33 ground-level measurements and model simulations has confirmed the high quality of the
34 measurements, with a high signal to noise ratio, indicating the usefulness of the data collected
35 (Borsdorff, 2018a, 2018b; Schneising et al., 2019, 2020).

36 In this study, we make use of carbon monoxide (CO) observations from TROPOMI (see Sect.
37 2.1) and the surface measurement network to investigate different regional sources of CO in
38 terms of their contribution to the total column and surface-level concentrations during high
39 pollution episodes in the winter season. By comparing CO measurements with high-resolution
40 model simulations generated by WRF-Chem-GHG, we aim to understand the contribution of
41 different sources to the observed CO enhancement. In particular, we focus on CO enhancement
42 caused by the emissions from both biomass burning and anthropogenic activities and their



1 relative roles in the severe air pollution of major cities nearby. This paper aims to address the
2 following questions: 1) How large is the CO enhancement over northern India detected by
3 TROPOMI during the agricultural stubble burning period? 2) What is the regional contribution
4 of CO emissions over India during the entire year 2018? 3) How good is the agreement
5 between the WRF-Chem-GHG and the observations both at ground level and integrated across
6 the column? 4) How does the column respond to the spatio-temporal variations of surface
7 emissions, particularly biomass emissions? and 5) What is the role of different emission
8 sources in terms of their contribution to the enhanced concentration level during the high
9 pollution episodes over India? An analysis focusing on identifying the sources contributing to
10 the high pollution event in North India during November 2017 using WRF modelling and
11 TROPOMI preliminary operational data was reported in Dekker et al., 2019, but here we
12 present the analysis for the succeeding year, i.e. November 2018, which also differs from the
13 previous study as follows: the present study (1) uses the retrievals from both WFM-DOAS
14 (Schneising et al., 2019, see Sect. 2.1) and TROPOMI/SICOR algorithms (Landgraf et al.,
15 2016) (2) examines the regional distribution of CO for the entire year, (3) employs different
16 model configuration such as model domain size, vertical eta levels, and planetary boundary
17 layer scheme, (4) prescribes a different anthropogenic emission inventory that also includes
18 hourly variations, and (5) utilizes the entire month, which includes biomass burning and non-
19 biomass burning periods to get a more detailed view of the dispersion to nearby places.

20 **2. Data**

21 **2.1. TROPOMI column observations**

22 The Tropospheric Monitoring Instrument (TROPOMI), onboard the Sentinel 5-Precursor
23 satellite (S5P), has been measuring various trace gases, including CO since November 2017
24 (Landgraf et al., 2016; Borsdorff et al., 2018a, 2018b; Schneising et al., 2019, 2020). The
25 TROPOMI instrument consists of a shortwave infrared nadir viewing imaging spectrometer,
26 which measures radiances around 2.3 μm wavelength, from which the total column mixing
27 ratio (XCO) is retrieved (Schneising et al., 2019; Landgraf et al., 2016). Due to the wide swath
28 of about 2600 km, the instrument is able to cover the whole globe on a daily basis, capturing
29 full scenes of continuous observations in cloud-free conditions (Schneising et al., 2019, 2020).
30 As a result of the observation of reflected solar radiation in the SWIR part of the solar
31 spectrum, TROPOMI yields atmospheric carbon monoxide measurements with high sensitivity
32 to all altitude levels including the planetary boundary layer and is thus well-suited to study
33 emissions from fires (Schneising et al., 2020).

34

35 For this study, we use TROPOMI CO data for November 2018 retrieved using the scientific
36 algorithm, the Weighting Function Modified Differential Optical Absorption Spectroscopy
37 (WFM-DOAS) optimised to retrieve vertical columns of carbon monoxide and methane
38 simultaneously (Schneising et al., 2019). Additionally, we use TROPOMI operational data
39 (TROPOMI/SICOR CO, Borsdorff et al., 2018a, 2019b) to examine the consistency of these
40 two observational products over India. The SICOR and WFMD-DOAS algorithms differ in
41 many aspects including radiative transfer models, inversion schemes and the quality filtering



1 method used. Whereas WFMD retrievals are limited to cloud free scenes, SICOR aims to
2 retrieve CO columns for cloudy ground pixels also. A global comparison between these two
3 datasets from December 2018 (Schneising et al., 2019) shows a very similar spatial CO pattern
4 for both algorithms with a high correlation coefficient of 0.98 and a regression factor close to
5 the 1:1 line, confirming good agreement between the two datasets. An overview of the
6 TROPOMI datasets used in this study is provided in Table 1 and additional details are provided
7 in the following two sub-sections.

8 **2.1.1. Scientific TROPOMI WFMD CO product**

9 The WFM-DOAS retrieval algorithm was initially developed for the SCIAMACHY instrument
10 onboard the ENVISAT satellite (Buchwitz et al., 2006, 2007; Schneising et al., 2011, 2014)
11 and has recently been adjusted for XCO retrieval from TROPOMI (Schneising et al., 2019,
12 2020). WFMD-DOAS uses a least squares approach, which retrieves XCO from the shortwave
13 infrared spectra recorded by the TROPOMI instrument. The TROPOMI WFMD CO retrievals
14 (referred as WFMD hereafter) have undergone direct validation with independent reference
15 data from the worldwide total carbon column observing network (TCCON, Wunch et al., 2011)
16 which consists of ground-based Fourier transform spectrometer (FTS) instruments with a well-
17 controlled light path. TCCON measurements are calibrated to the World Meteorological
18 Organization (WMO) scale. As per this validation, WFMD XCO has a systematic error of 1.9
19 ppb and a random error of 5.1 ppb (Schneising et al., 2019).

20 **2.1.2. Operational TROPOMI/SICOR CO product**

21 The operational TROPOMI/SICOR CO product (referred to as SICOR hereafter) is retrieved
22 using the Shortwave Infrared Carbon Monoxide Retrieval (SICOR) algorithm (Landgraf et al.,
23 2016; Borsdorff et al., 2018a, 2018b). The validation study of SICOR with the CAMS data
24 show a good agreement with global mean difference of +3.2% and a Pearson correlation
25 coefficient of 0.97 (Borsdorff et al., 2018b) and for the Indian region, a 2.9% difference was
26 found with CAMS with a standard deviation of 6% and a Pearson correlation coefficient of 0.9
27 (Borsdorff, 2018a). As per the validation of SICOR with ground-based total column
28 measurements of TCCON, a mean bias of 6 ppb with a standard deviation of 3.9 ppb and 2.4
29 ppb has been found for clear and cloudy skies respectively (Borsdorff, 2018a).

30 **2.2. Ground-level observations**

31 To assess the model performance against the surface level measurements, we use
32 measurements from ground-based air quality monitoring network maintained by the Central
33 Pollution Control Board (CPCB) of India. The measurements of CO are performed using CO
34 analysers based on non-dispersive infrared spectroscopy, and the data are provided as 6-hour
35 averages via a publicly-accessible online portal ([https://app.cpcbcr.com/ccr/#/caaqm-](https://app.cpcbcr.com/ccr/#/caaqm-dash-board-all/caaqm-landing/data)
36 [dash-board-all/caaqm-landing/data](https://app.cpcbcr.com/ccr/#/caaqm-dash-board-all/caaqm-landing/data)). Though we have analysed CO measurements available
37 from all stations for the period of 3-20 November 2018, measurement stations that are too close
38 to local emissions sources showing extremely large and ambiguous variations in which stability
39 of the analyser may be questioned, were excluded for the evaluation. All the stations used for
40 this evaluation are listed in Table 2.



1 3. WRF-Chem-GHG model

2 We utilize a high-resolution modelling framework based on a WRF-Chem-GHG (version
3 3.9.1.1, hereafter referred to as WRF) for simulating CO concentrations at a spatial resolution
4 of 10 km × 10 km) and a temporal resolution of 1 hour. The model solves the compressible
5 Euler non-hydrostatic equations and uses a terrain-following hydrostatic pressure coordinate
6 system in the vertical direction (Skamarock et al., 2008). In our case, simulations have 39
7 vertical levels extending from the surface to 50 hPa (~20 km) and the model domain describes
8 a region with a spatial extent of 3500 km × 2500 km, covering the Indian domain and some
9 parts of Bangladesh, China, Nepal and Pakistan.

10 For meteorological initial and boundary conditions, we have taken ECMWF ERA5 data on an
11 hourly basis with a horizontal resolution of 0.25° × 0.25°. For CO concentration fields, initial
12 and boundary conditions are prescribed from the Copernicus Atmosphere Monitoring Service
13 (CAMS re-analysis data). CAMS provides the estimated mixing ratios of CO with a spatial
14 resolution of 0.25° × 0.25° at a temporal resolution of 6 hours on 60 vertical levels. For CO
15 simulations, we have mainly used anthropogenic and biomass burning emissions tracers from
16 external datasets. To represent anthropogenic contributions, we use the global EDGAR
17 emission inventory (Emission Database for Global Atmospheric Research, version 4.3.2, the
18 year 2012) data at a spatial resolution of 0.1° × 0.1°. EDGAR provides global inventories for
19 GHG emissions and air pollutants on an annual basis, but we apply time factors in order to
20 create hourly emissions. The time factors are based on the step-function time profiles published
21 on the former EDGAR website: [http://themasites.pbl.nl/images/temporal-variation-](http://themasites.pbl.nl/images/temporal-variation-TROTREP_POET_doc_v2_tcm61-47632.xls)
22 [TROTREP_POET_doc_v2_tcm61-47632.xls](http://themasites.pbl.nl/images/temporal-variation-TROTREP_POET_doc_v2_tcm61-47632.xls) (see Kretschmer et al., 2014; Steinbach et al.,
23 2011, for further details). We use the CO emission data from the Global Fire Assimilation
24 System (GFAS) for the year of 2018 to represent biomass burning emissions. GFAS is a
25 satellite-based fire emission inventory (<http://apps.ecmwf.int/datasets/data/cams-gfas/>), which
26 provides biomass-burning emissions daily at a global horizontal resolution of 0.1° × 0.1°. The
27 inventory calculates the fire emissions by assimilating fire radiative power (FRP) observations
28 from MODIS instruments on the polar-orbiting satellites Aqua and Terra, which observe the
29 thermal radiation from fire activities at wavelengths around 3.9 μm and 11 μm (Kaiser et al.,
30 2012). It achieves higher spatial and temporal (daily) resolution than almost any other
31 inventory and can estimate near-real-time emissions. A number of studies have reported the
32 underestimation of GFAS in fire emissions due to the limitations of the MODIS instruments,
33 which do not capture all of the biomass burning emissions (Cusworth et al., 2018; Dekker et
34 al., 2019; Huijnen et al., 2016; Kaiser et al., 2012; Mota and Wooster, 2018).

35 All these emissions fluxes are gridded to WRF's Lambert conformal conic projection grid with
36 10 km horizontal resolution, conserving the total mass of emissions. These fluxes are added to
37 the first model layer and transported separately as tagged tracers (Pillai et al., 2016). In order
38 to account for the CO transported from the boundaries, we used CAMS CO data derived at the
39 boundary conditions and refer to this CO tracer as "background", meaning the concentration
40 without considering any sources or sinks in the targeted domain. The total CO is then
41 calculated as: CO total = CO background (BCK) + CO anthropogenic (ANT) + CO biomass
42 (BBU).



1 Utilizing the emission tracers mentioned above as well as the multiple physics and chemistry
2 options and dynamics schemes, model simulations of CO are performed for the period 01–30
3 November 2018. The model setup does not include the deposition and chemical formation of
4 CO from volatile organic compounds (VOCs). Compared to the direct CO sources such as
5 anthropogenic and biomass burning emissions over the model domain, the indirect source from
6 VOC oxidation is much smaller, and the deposition processes are minor compared to the
7 transport of CO out of the model domain (Dekker et al., 2017). Also, the oxidation with the
8 hydroxyl (OH) radical is not considered. Based on a few sensitivity simulations, Dekker et al.,
9 (2017) reported a slight (4%) net decrease of enhancement when including chemical reactions
10 of CO and concluded that the CO enhancement pattern is hardly affected by VOCs and OH
11 oxidation.

12 4. Methods

13 4.1. Comparison of WRF simulations with satellite column observations

14 To evaluate the performance of WRF, we have performed a comparison study on a daily and
15 monthly basis using WFMD column CO (XCO) data during the period 1-30 November 2018
16 over the Indian domain. The WFMD dataset also provides the column averaging kernel vector
17 (AK), describing the vertical sensitivity of the retrieved CO column to the partial column at
18 different vertical levels (Schneising et al., 2019). In order to compare the satellite data with
19 model simulations quantitatively, we have to use the AK to take into account the vertical
20 sensitivity of the instrument. In the dataset, the elements of the AK mostly have values close to
21 1, meaning that the instrument is sensitive to the full column of CO. As such, the prior
22 estimates have a negligible contribution to the retrieved columns. To compare the simulated
23 concentration fields with the satellite observations, the simulated pressure-weighted column-
24 averaged dry air mole fraction after applying the averaging kernel, c_{avgk} is calculated as
25 follows:

$$26 \quad c_{avgk} = c + \frac{1}{m_0} + \sum_{l=1}^n (m_l(1 - A_l) (x_T^l - x^l)) \quad \text{Eq. 1}$$

27
28 In this equation, l is the index of the vertical layer and n is the number of vertical layers, and A_l
29 the corresponding column-averaging kernel of the WFMD algorithm. c is the pressure-
30 weighted column averaged dry air mole fraction calculated from model simulations. x_T is the a
31 priori dry air mole fraction profile used by the WFMD retrieval algorithm, which is also
32 provided in the data product, and x is the model simulation. m_l is the mass of dry air for the
33 corresponding layer and m_0 is the total mass of dry air. For the comparison, we used only
34 WRF simulations that correspond to the satellite sampling time. For a fair comparison between
35 the satellite observations and model simulations, the averaging kernel matrix and a priori
36 profile for each retrieval have been applied to the corresponding model output as explained in
37 Eq. 1. For the ease of the statistical analysis, the observations, though comparable to the model
38 resolution, are gridded to the WRF spatial resolution of $10 \text{ km} \times 10 \text{ km}$. Both WFMD and
39 WRF averaged data for the month of November and a period of 6-9 November (enhanced
40 biomass burning period as per the GFAS data) are utilized in this study to investigate the



1 column enhancement by fire CO and their distribution over the study domain. During the
2 enhanced biomass-burning period, a definite enhancement in XCO is found over the biomass
3 burning hotspot. The monthly averaged map shows decreased concentration levels over these
4 hotspots, which is attributed to the CO concentration dispersion resulted by changing weather
5 conditions.

6 **4.2. Comparison of WRF simulations with ground-level observations**

7 To evaluate the model performance at surface level, we have performed a comparison study
8 with the CO in situ measurements obtained from the ground-level pollution measurement
9 stations. We use the data collected from 20 measurement stations within the IGP region and
10 evaluation is done against each station data. In order to see overall agreement for different
11 regions in the IGP, we have averaged the data temporally using only the stations within the
12 corresponding regions (Delhi, Punjab, and the IGP). The entire month is not used here due to
13 the existence of data gaps from several stations. In order to avoid very localised influence and
14 noise in the observed data, the 1-hourly datasets are temporally averaged to 6-hourly
15 resolution.

16 **5. Results and Discussions**

17 **5.1. Regional and seasonal variation of fire CO emission**

18 In order to examine the spatio-temporal variations of the monthly fire CO emission, we have
19 divided the entire region into five sub-regions as shown in Fig. 1. The fire CO emissions show
20 significant spatial and temporal variations, with predominant emissions over the Indo-Gangetic
21 Plain (IGP), Central India (CI), and northeast India (NEI).

22 Figure 2 illustrates the integrated monthly fire CO emission for those regions in 2018. In most
23 parts of India, the fire CO emissions peak during the March-April (pre-monsoon) period,
24 accounting for about 76% of the annual emissions. This is consistent with a study based on the
25 fire counts analysis from 1998-2009, which reported that more than 75% of the annual fires
26 occurred during March-April (Sahu et al., 2015). Fire CO emissions during March are
27 significantly higher when compared to other months, accounting for about 55% of the annual
28 emissions for India. Although having a small geographical area, the fire activities over
29 northeast India (NEI) made a significant contribution (57%) to emissions during pre-monsoon
30 months, while the IGP contributed only about 5%. Central (CI) and southern regions (SI) of
31 India add about 33% towards the pre-monsoon fire CO emissions, while North India (NI)
32 shows fewer emissions during the whole year. However, emission spikes are seen in the IGP
33 during the October-November (post-monsoon) period. Over the IGP, the fire CO emissions
34 show evident monthly variations with a higher emission during the post-monsoon time
35 compared to the pre-monsoon period. About 73% of the country's total fire CO emissions
36 during the post-monsoon period are from the IGP region. Of these IGP post-monsoon
37 emissions, 70% come from the northwest states of the IGP: Punjab and Haryana. Over this
38 region, 25% of the total fire CO emissions happened within a short period during 6-9
39 November, which accounts for about 18% of the country's post-monsoon total fire CO
40 emissions. During the monsoon time, all regions are found to have fewer fire emissions, which



1 can be attributed to the fact that rainfall leads to suppressed fire activity. In addition to the
2 minimal possibility of fire activities during the rainy season, note that MODIS has only a
3 limited capability to detect fire emissions over a cloudy scene.

4 The observed monthly variations in fire emissions are mainly due to factors such as post-
5 harvest crop residue burning, meteorological conditions (dry weather), and land-use practices
6 (Habib et al., 2006). The fire activities during post and pre-monsoon periods in India are
7 mostly associated with the high-level crop residue burning during the post-harvest seasons
8 (Sahu et al., 2015). Crop residue burning after harvesting is a general practice used by farmers
9 to make the land clear for the next crop. Over the IGP, there are mainly two seasonal crop
10 seasons known as Kharif (primarily rice), and Rabi (mainly wheat), which are harvested during
11 post and pre-monsoon seasons respectively (Sahu et al., 2015). This results in the temporal
12 variations of residue burning emissions over the IGP. Compared to other parts of the IGP, the
13 northwest part of the IGP has the greatest preponderance of crop residues during the post-
14 monsoon season (Singh and Panigrahy, 2011). Consistent with the spatial and seasonal
15 differences in agricultural practices, we see a high level of fire CO emissions in this region
16 during the short period of 6-9 November.

17 **5.2. Enhanced XCO as observed by the satellite**

18 Figure 3(a) shows the column CO dry mixing ratio retrieved from WFMD over the Indian
19 domain averaged for the entire month of November and November 6-9 (most intense biomass
20 burning period). During this period, higher values of column CO are observed over the
21 northern part of India, particularly over the IGP region, compared to the other regions of India,
22 showing higher values during the biomass burning period than the monthly average. A distinct
23 enhancement in XCO can be observed during the biomass-burning period specifically over the
24 state of Punjab and Haryana, with a distribution plume towards the southeast direction
25 including the region of Delhi and Agra. Note that this emission hotspot is also seen in the
26 GFAS inventory during the biomass-burning period (Fig 2). Consistency between the GFAS
27 inventory and satellite observations suggest that the XCO enhancement over the northwest part
28 of the IGP during 6-9 November can be attributed to the crop residue burning that occurred
29 over the Punjab region. The consistency check between two retrieval products (WFMD and
30 SICOR) has resulted in a very similar spatial CO pattern for both algorithms with a high
31 correlation coefficient of 0.97 confirming the robustness of our findings between the two
32 datasets over India (see Table 3). During early winter (November and December), the shallow
33 PBL and low wind speed cause locally-emitted gases to be trapped in the lower atmosphere,
34 which is considered to be the primary cause for high concentrations during this period. For a
35 better understanding of the role of transport and CO emissions from biomass burning to the
36 distribution over the domain, we utilized WRF model simulations and performed a comparison
37 study with the WFMD observations as explained in Sect. 4.1.

38 **5.3. Validation of WRF**

39 **5.3.1. Agreement with column observations**



1 We compared WRF simulations with WFMD observations, averaged over the days of peak
2 burning and over the full month of November 2018. Fig. 3 demonstrates these comparisons.
3 Both satellite and the model show a higher level of column CO over the IGP region than over
4 any other region of the domain. In the monthly averaged plots, the model slightly overestimates
5 (by about 10 ppb) the XCO in most parts of the domain. Between the monthly averaged
6 observations and the simulations, we find a mean difference of 7 ppb with a standard deviation
7 of 8 ppb and a correlation coefficient of 0.87 (Fig. 4).

8 During the biomass-burning period, the model underestimates (by about 10-15 ppb) the
9 enhancement over Punjab and some central parts of Uttar Pradesh while overestimating (by
10 about 15-20 ppb) enhancements over the eastern parts of IGP including West Bengal and some
11 parts of Bihar. Fig. 4 demonstrates these differences. Daily retrievals of WFMD and
12 corresponding simulations for the biomass-burning period are shown in Fig. 5. An enhanced
13 XCO is reported in both observations and simulations over the state of Punjab, starting from 6
14 November and gradually increases in the following days. During this period, the plume is seen
15 to be partly transported in a southeast direction along the region of Delhi and Agra. Over the
16 IGP, there exists an overall slight underestimation by WRF in comparison to TROPOMI during
17 this period with a mean model-to-observation difference of -2.7 ppb.

18 Figure 6 shows the temporal evolution of the CO concentration in three cities (Barnala, New
19 Delhi, and Agra) located along the transport pathway of pollution. The data are averaged in a
20 100 km x 100 km square around the centre of each city. During the biomass-burning period,
21 the XCO over Barnala (Punjab) shows a steady positive increment with time with a peak on 9
22 November with a value of approximately 165 ppb. Both observations and simulations suggest a
23 southeast transport of this plume that increases the CO concentration over Delhi and Agra
24 during 8 and 9 November. Over Delhi, the WFMD XCO reached a maximum on 8 November
25 while modelled CO showed a delay, with a maximum concentration on 9 November. On 9
26 November, observation shows more dispersed XCO over Delhi towards the southeast direction
27 in comparison with model simulations. Over Agra, which is located far away from the
28 pollution hotspot but along the transport pathway, an increase in XCO, which is consistent with
29 that over the other two cities is found. The details in Table 3 confirm the minimal impact of
30 differences in satellite retrieval algorithms on our results. This analysis suggests a promising
31 usage of TROPOMI observations to understand the details of hotspot emissions and the
32 distribution of transport. The model is able to capture many of these spatial and temporal
33 patterns, supporting the potential use of WRF via inverse modelling to infer hotspot emissions
34 using column measurements.

35 **5.3.2. Agreement with ground-level observations**

36 Figure 7 shows the model evaluation with ground-level measurements over the regions IGP,
37 Delhi and Punjab for a period from 3 to 20 November 2018. The location of ground-level
38 measurement stations used for this study is shown in Fig. 8. The entire month is not used here
39 due to the existence of data gaps from several stations. Taking various ground-based stations
40 over the IGP, Delhi and Punjab, we see an overall good agreement between model and
41 measurements, with a correlation coefficient of 0.6 (for the IGP), 0.6 (Delhi) and 0.41



1 (Punjab). Among these three study regions, a lower correlation is found for the Punjab region
2 in which measurement sites are very close to the biomass burning hotspots, therefore showing a
3 larger variability compared to other stations. These variations are not fully reproduced by the
4 model, resulting in lower correlations over Punjab region. Though the model is able to follow
5 the temporal variation in the surface level CO concentrations, overall underestimations of 9
6 ppb and 54 ppb are found for Punjab and Delhi. For the IGP region, the model underestimates
7 the observed enhancements considerably, resulting in a mean bias of 162 ppb. The observed
8 underestimation of WRF can be attributed to the local source enhancements at the ground-level
9 stations, which are closely located to the cities. For the Punjab region, the model CO surface
10 concentration shows the influence of biomass burning starting from 6 November with a
11 maximum of 800 ppb on 8 November. Unlike the Punjab region, the concentration patterns
12 over Delhi and the IGP show a steadily increasing trend from 6 to 13 November, with a
13 subsequent reduction in mixing ratios for the remaining days. Among these study regions
14 during this period, the lowest and highest surface CO levels are observed over the regions
15 Punjab (mean: 500 ppb) and Delhi (mean: 1500 ppb) respectively. Except for Punjab, we see
16 better mean bias when excluding nighttime values (21 ppb for Delhi and 141 ppb for the IGP
17 region), as the uncertainty from mixing height simulations is larger during nighttime compared
18 to daytime. Surprisingly the overall underestimation increased in Punjab when using only
19 daytime values, indicating a considerable underestimation of local emission sources, likely
20 from the biomass emission inventory. Note that the GFAS fire emissions may be
21 underestimated (Mota and Wooster, 2018). The GFAS fire emissions are partly based on the
22 MODIS satellite instrument, and the limited resolution of the instrument misses many small
23 fires, including biomass burning over India (Cusworth et al., 2018). Overall, the results show
24 that the model simulation at a high spatial resolution is capable of capturing the CO
25 enhancement and reduction pattern at most of the stations, however there is a non-trivial mean
26 bias which can be attributed to issues with simulating transport and PBL dynamics in WRF as
27 well as the variability in emission fluxes which is likely to be not sufficiently well represented
28 in the emission inventories used.

29 **5.4. Contribution of different sources to the observed concentration**

30 To further investigate the contribution of different emission sources to the observations, we use
31 the “tagged-tracer” option in WRF and separate the contributions from different sources as
32 shown in Fig. 6 and 7. Note that the signals contributing to satellite observations are difficult to
33 disentangle without underlying assumptions or the availability of multi-tracers such as CO and
34 NO_x and NO_y^* (NO_y^* includes NO_x , PAN, organic nitrates, HNO_3 , and N_2O_5 , e.g. Wang et al.,
35 2002). The relative contributions of different emission sources and processes to the WRF CO
36 column, as summarized in Table 4, clearly indicate the dominance of anthropogenic signals
37 over biomass burning signals on the XCO enhancements. The significant impact of background
38 signal owing to the advection from the domain boundary throughout the column indicates the
39 influence of far-field fluxes and large-scale transport patterns on column CO (see Fig. 6).
40 During the biomass-burning period, there exists a considerable contribution of biomass burning
41 emissions to the column mixing ratios particularly over the Punjab region (14%). Relatively
42 low contributions of biomass burning signals to the column in Delhi and the IGP compared to



1 Punjab indicates the dominant contribution of surface CO emission to the column in Punjab
2 where the biomass emissions originated. It also suggests the possibility of less dilution of
3 surface emissions during wintertime, enhancing the total column mixing ratios. The effect of
4 advected biomass burning signals in terms of their contribution to the column can be seen over
5 Delhi (12%), however this effect becomes smaller in the IGP (5%) due to further dispersion.

6 The diurnal variation in the surface level CO concentration pattern is due to the diurnal
7 variation in the planetary boundary layer height (PBLH) combined with strong sources of CO
8 at the surface. The contribution from emissions sources over the Delhi, the IGP and Punjab
9 regions for the period of 3-20 and specifically 6-9 November are also summarised in Table 4.
10 For all regions, the influence of background CO concentrations to the observed variability is
11 minimal, as expected (see Fig. 7). The background influence is expected to be smaller for
12 surface CO in urban areas where the CO fraction from local anthropogenic emissions
13 dominates over the background signals. At ground level in Delhi and the IGP, a detectable
14 enhancement in surface CO due to fire CO is found only during 6-9 November. During this
15 period, the average contribution of biomass burning to the ground level concentration is 10%,
16 while the anthropogenic contribution is 79-83%. During 3-20 November over Delhi, however,
17 the average contribution from fire dropped to 4% compared to 85% in the case of the
18 anthropogenic contribution.

19
20 Overall, our findings suggest that the enhanced CO levels during pollution episodes over Delhi
21 and the greater part of IGP are affected by biomass burning. However, a more significant
22 contribution comes from anthropogenic emissions. Unlike the surface CO mixing ratios, the
23 majority of the column CO mixing ratio is contributed by the background signal. A recent
24 study conducted by Dekker et al., (2019) concluded that there exists an underestimation in
25 GFAS fire emission data over the Indian region, which is supported by our findings. However,
26 over the Punjab region, biomass burning played a significant role in determining the ground
27 level CO measurements, especially during 6-9 of November, during which enhanced fire
28 activities occurred. This has contributed considerably to the column mixing ratio that is
29 detected by TROPOMI. On average, for 3-20 of November, 17 % of the total ground level CO
30 concentration over the Punjab region are on account of fire CO emission, whereas for 6-9
31 November, the share is about 38%.

32 **5.5. Effect of meteorology**

33 Usually pollution episodes during winter are the result of meteorological conditions due to low
34 wind speed and shallow boundary layer (PBL height). Figure 9 demonstrates the influence of
35 the PBL height and surface-level wind speed to the observed CO level. We found a negative
36 correlation of CO with modelled PBLH (-0.83 (IGP), -0.73 (Delhi), -0.56 (Punjab)) and wind
37 speed (-0.62 (IGP), -0.40 (Delhi), -0.24 (Punjab)). A strong negative relation between PBL
38 height and CO level is seen, indicating the impact of meteorology on the diurnal variation of
39 surface-level CO concentration. Among the regions, a less negative correlation of CO with
40 PBLH and wind speed is observed for Punjab. It suggests that when compared to Delhi and the
41 IGP, the surface level CO variation over the Punjab region cannot be explained by meteorology



1 alone: Here the local emission activities, such as biomass burning, explain more of the
2 variability in surface level CO.

3

4 A gradual increase in surface CO levels was observed from 3 to 13 of November during which
5 an overall decrease in PBL height and surface-level wind speed took place. The highest CO
6 values around Delhi were found during 11-13 November, just before the winds and PBL height
7 were increasing. The findings suggest that the meteorological conditions have a large impact
8 on the surface level CO concentration, especially over the IGP and Delhi. Our results are
9 consistent with Dekker et al. (2019), who identified that the meteorological conditions
10 contributed significantly to the enhancement of CO mixing ratios at the ground level during
11 November 2017. Similarly Kariyathan et al. (2020), by using a-temporal emission fields and a
12 Lagrangian modelling framework, found a considerable impact of meteorological conditions
13 during November 2017 that contributed to the enhancements of trace gases over Delhi.
14 Together with strong emissions (anthropogenic and biomass burning), they found that these
15 enhancements could be several orders of magnitude higher compared to other seasons.

16 **6. Conclusions**

17 The Tropospheric Monitoring Instrument (TROPOMI) on board ESA's Copernicus Sentinel-5
18 Precursor (S5P) mission provides shortwave infrared measurements of CO with daily global
19 coverage and a high spatial resolution of 7×7 km². These high density and high accuracy CO
20 column observations enable us to investigate high CO pollution episodes over India, which
21 otherwise would not have been possible at this spatial resolution. In this study, we demonstrate
22 the usefulness of TROPOMI CO column observations for detecting and analysing local CO
23 enhancement over India during winter 2018, employing WRF at a resolution comparable to
24 TROPOMI to aid in the interpretation of the data. The GFAS biomass burning emission
25 product shows a substantial amount of fire CO emitted from various parts of India during the
26 year 2018. Over the IGP, the fire CO emission shows an apparent monthly variation with a
27 higher emission during the post-monsoon time compared to the pre-monsoon period. A large
28 amount of fire CO emissions is reported over the state of Punjab within the short period of
29 November 6-9 2018. Consistent with the emission data, TROPOMI XCO shows a clear
30 enhancement during November not only over the fire emission hotspots but also along the
31 western parts of the IGP, including the national capital of India, Delhi.

32 For further analysing the causes of these enhancements, we used simulations generated by
33 WRF. A similar study conducted by Dekker et al., (2019) also utilized WRF for identifying the
34 sources contributing to the high pollution event in North India during 2017, but using
35 preliminary TROPOMI data generated with the SICOR algorithm. The present study uses both
36 fossil fuel emissions data based on EDGAR (version 4.3.2) with hourly variations and biomass
37 burning emissions data based on GFAS fire CO emissions.
38 If WRF reproduces the transport sufficiently well, the mismatch between the simulations and
39 observations is mostly caused by uncertainties in the prior emission fluxes (EDGAR and
40 GFAS) due to the linear dependence of the CO concentrations on the source strength of the
41 emissions. To evaluate the simulated CO fields with the observed CO columns, we applied
42 the WFMD averaging kernel to the corresponding model profile, taking into account the



1 vertical sensitivity of the satellite measurement. Overall, we find a good agreement between
2 WRF and WFMD with a mean difference of 7 ppb, a standard deviation of 8 ppb, and a spatial
3 correlation coefficient of 0.87.

4
5 Our analysis shows that daily observations from TROPOMI allow pollution transport from the
6 emissions hotspots to be captured. As an example, we analysed the pollution transport from the
7 fire emissions hotspots over northern India during the enhanced burning period of November 6-
8 9. WFMD XCO level started to rise over the fire emission hotspots from 6 November and
9 gradually increased during the following days. Both WFMD and model simulations show the
10 transport of CO polluted air masses towards the northeast part of the IGP along with the capital
11 city Delhi. Due to this pollution transport, the CO concentration level in the cities along the
12 transport pathway shows CO enhancements. A similar transport pattern is also observed in our
13 WRF model simulation. This supports the reliability of WRF transport simulation and suggests
14 the potential of using WRF to estimate CO emission via flux inversions. The good agreement
15 between WFMD and SICOR retrievals over India confirms the robustness of our findings
16 irrespective of the differences in the retrieval algorithm.

17
18 For the further evaluation of WRF with surface measurements, we used ground level CO
19 measurements from the stations along the IGP for the period of 3-20 November 2018. The
20 comparison shows a good agreement between simulations and observations with a correlation
21 coefficient of 0.6 (for the IGP), 0.6 (Delhi) and 0.41 (Punjab). Over these regions, the surface
22 CO showed a steady increasing trend from 6 to 13 November, followed by a reduction in
23 mixing ratio in the following days. Among these study regions, the lowest and highest surface
24 CO level was observed over the regions Punjab and Delhi respectively.

25
26 Overall, our results imply a minimal role of biomass burning in terms of its contribution to
27 both column and surface enhancements compared to other anthropogenic sources, except for
28 the state of Punjab during the high pollution episodes. This is also consistent with Dekker et al.
29 (2019), which concluded that the low wind speeds and shallow atmospheric boundary layers
30 were the most likely causes for the temporal accumulation and subsequent dispersion of CO
31 during the biomass-burning period in November 2017. By comparing our results with Dekker
32 et al. (2019), we can infer the significant role of atmospheric dynamics and anthropogenic
33 emissions on producing exorbitant level of pollutants and trace gases during every winter in
34 northern India. While these anthropogenic urban sources (e.g. road traffic, residential air-
35 conditioning systems, industries and power plants) are primarily responsible for the CO
36 enhancement in winter months, there exists a non-trivial fraction of contribution from biomass-
37 burning activities in Punjab and nearby locations for a short duration of time. The variation in
38 surface-level CO concentrations is found to be influenced significantly by the meteorological
39 parameters such as PBL height and surface level wind speed. Our results show a clear
40 influence of atmospheric transport leading to a complex CO enhancement pattern. This
41 demonstrates the need for high-resolution models in the interpretation of TROPOMI
42 observations in order to get more insight into the pollution transport and deduce causes for the
43 observed enhancements (and resulting poor air quality) over India.



1
2 In an effort towards minimizing the pollution episodes, a robust evaluation of emissions
3 inventories and their trends is vital, particularly in light of uncertainties in existing emission
4 sources, and the limited availability of appropriate emissions estimates in different emission
5 sectors. Studies identifying the emissions hotspots and understanding their transport patterns
6 such as that carried out in Dekker et al. (2019) and in this work are thus important for further
7 decision making for emission control. While WRF is able to reproduce observations reasonably
8 well, the model errors are not negligible when utilizing TROPOMI observations for emission
9 estimates. Nevertheless, we emphasize the importance of taking rigorous policy measures to
10 reduce residential and commercial emissions in addition to measures already being taken in the
11 agricultural sectors (e.g. the implementation of second-generation direct-seeders, such as the
12 Happy Seeder, which facilitate sowing under heavy stubble conditions, thereby avoiding the
13 need for residue burning, NAAS, 2017). The future task involves the implementation of
14 appropriate inverse techniques suitable for flux inversion of spatially resolved sources of CO
15 emissions over India.
16



1 **Code/Data availability**

2 The WRF-CO model simulations used in this study are available upon request to the
3 corresponding author D. Pillai (dhanya@iiserb.ac.in, kdhanya@bgc-jena.mpg.de). The WRF-
4 Chem source code is publicly available (<https://ruc.noaa.gov/wrf/wrf-chem/>). The input data
5 used for simulations in this study are either publicly available or available upon request to D.
6 Pillai. The S5P WFM-DOAS data can be accessed from [http://www.iup.uni-
7 bremen.de/carbon_ghg/products/tropomi_wfmd/](http://www.iup.uni-bremen.de/carbon_ghg/products/tropomi_wfmd/) and the operational product is available at
8 <https://scihub.copernicus.eu/>. The ground-based CO data analysed in this study can be
9 accessed from <https://app.cpcbcr.com/ccr/#/caaqm-dashboard-all/caaqm-landing/data>.

10 **Author Contribution**

11 DP designed the study and performed the model simulations. AV and DP interpreted the
12 results. AV performed the TROPOMI/WFMD and in-situ data analysis, and wrote the paper.
13 JM, CG, MB, and OS provided significant input to the interpretation, and the improvement of
14 the paper. All authors discussed the results and commented on the paper.

15 **Competing interests**

16 The authors declare they have no conflict of interest.

17 **Acknowledgements**

18 This study is supported by the funding from the Max Planck Society allocated to the Max
19 Planck Partner Group at IISERB. We acknowledge the support of IISERB's high performance
20 cluster system for computations, data analysis and visualisation. The WRF-Chem simulations
21 were done on the high performance cluster Mistral of the Deutsches Klimarechenzentrum
22 GmbH (DKRZ). The first author acknowledges the research infrastructure support provided by
23 IISERB and thanks Thara Anna Mathew and Monish Deshpande for their contribution to
24 graphics.



1 **References**

- 2 Akagi, S. K., Yokelson, R. J., Wiedinmyer, C., Alvarado, M. J., Reid, J. S., Karl, T., Crouse,
3 J. D. and Wennberg, P. O.: Emission factors for open and domestic biomass burning for use in
4 atmospheric models, *Atmos. Chem. Phys.*, 11(9), 4039–4072, doi:10.5194/acp-11-4039-2011,
5 2011.
- 6 Andreae, M.O. and Metlet, P.: Emission of trace gases and aerosols from biomass burning,
7 *Global Biogeochem. Cycles*, 15(4), 955–966, 2001.
- 8 Andreae, M. O.: Emission of trace gases and aerosols from biomass burning – An updated
9 assessment, *Atmos. Chem. Phys. Discuss.*, 1–27, doi:10.5194/acp-2019-303, 2019.
- 10 Bond, T. C.: A technology-based global inventory of black and organic carbon emissions from
11 combustion, *J. Geophys. Res.*, 109(D14), D14203, doi:10.1029/2003JD003697, 2004.
- 12 Borsdorff, T.: Measuring Carbon Monoxide With TROPOMI : First Results and a Comparison
13 With ECMWF-IFS Analysis Data, *J. Geophys. Res.* , doi:10.1002/2018GL077045, 2018a.
- 14 Borsdorff, T., Aan De Brugh, J., Hu, H., Hasekamp, O., Sussmann, R., Rettinger, M., Hase, F.,
15 Gross, J., Schneider, M., Garcia, O., Stremme, W., Grutter, M., Feist, Di. G., Arnold, S. G., De
16 Mazière, M., Kumar Sha, M., Pollard, D. F., Kiel, M., Roehl, C., Wennberg, P. O., Toon, G. C.
17 and Landgraf, J.: Mapping carbon monoxide pollution from space down to city scales with
18 daily global coverage, *Atmos. Meas. Tech.*, 11(10), 5507–5518, doi:10.5194/amt-11-5507-
19 2018, 2018b.
- 20 Buchwitz, M., De Beek, R., Noël, S., Burrows, J. P., Bovensmann, H., Schneising, O.,
21 Khlystova, I., Bruns, M., Bremer, H., Bergamaschi, P., Körner, S. and Heimann, M.:
22 Atmospheric carbon gases retrieved from SCIAMACHY by WFM-DOAS: Version 0.5 CO and
23 CH₄ and impact of calibration improvements on CO₂ retrieval, *Atmos. Chem. Phys.*, 6(9),
24 2727–2751, doi:10.5194/acp-6-2727-2006, 2006.
- 25 Buchwitz, M., Khlystova, I., Bovensmann, H. and Burrows, J. P.: Three years of global carbon
26 monoxide from SCIAMACHY: Comparison with MOPITT and first results related to the
27 detection of enhanced CO over cities, *Atmos. Chem. Phys.*, 7(9), 2399–2411, doi:10.5194/acp-
28 7-2399-2007, 2007.
- 29 Crutzen, P. J. and Andreae, M. O.: Biomass Burning in the Tropics: Impact on Atmospheric
30 Chemistry and Biogeochemical Cycles, *Science* (80-.), 250(4988), 1669–1678,
31 doi:10.1126/science.250.4988.1669, 1990.
- 32 Cusworth, D. H., Jacob, D. J., Sheng, J. X., Benmergui, J., Turner, A. J., Brandman, J., White,
33 L. and Randles, C. A.: Detecting high-emitting methane sources in oil/gas fields using satellite
34 observations, *Atmos. Chem. Phys.*, 18(23), 16885–16896, doi:10.5194/acp-18-16885-2018,
35 2018.
- 36 Dekker, I. N., Houweling, S., Aben, I., Röckmann, T., Krol, M., Martínez-Alonso, S., Deeter,
37 M. N. and Worden, H. M.: Quantification of CO emissions from the city of madrid using



- 1 MOPITT satellite retrievals and WRF simulations, *Atmos. Chem. Phys.*, 17(23), 14675–14694,
- 2 doi:10.5194/acp-17-14675-2017, 2017.

- 3 Dekker, I. N., Houweling, S., Pandey, S., Krol, M., Röckmann, T., Borsdorff, T., Landgraf, J.
- 4 and Aben, I.: What caused the extreme CO concentrations during the 2017 high-pollution
- 5 episode in India?, *Atmos. Chem. Phys.*, 19(6), 3433–3445, doi:10.5194/acp-19-3433-2019,
- 6 2019.

- 7 Gamnitzer, U., Karstens, U., Kromer, B., Neubert, R. E. M., Meijer, H. A. J., Schroeder, H. and
- 8 Levin, I.: Carbon monoxide: A quantitative tracer for fossil fuel CO₂?, *J. Geophys. Res.*
- 9 *Atmos.*, 111(22), 1–19, doi:10.1029/2005JD006966, 2006.

- 10 Girach, I. A. and Nair, P. R.: Carbon monoxide over Indian region as observed by MOPITT,
- 11 *Atmos. Environ.*, 99, 599–609, doi:10.1016/j.atmosenv.2014.10.019, 2014.

- 12 Guenther, A., Karl, T., Harley, P., Weidnmyer, C., Palmer, P. I. and Geron, C.: Edinburgh
- 13 Research Explorer Estimates of global terrestrial isoprene emissions using MEGAN (Model of
- 14 Emissions of Gases and Aerosols from Nature) and Physics Estimates of global terrestrial
- 15 isoprene emissions using MEGAN (Model of Emissions of Gases an, *Atmos. Chem. Phys.*,
- 16 (6), 3181–3210, doi:10.5194/acp-6-3181-2006, 2006.

- 17 Gupta, P. K., Sahai, S., Singh, N., Dixit, C. K., Singh, D. P., Sharma, C., Tiwari, M. K., Gupta,
- 18 R. K. and Garg, S. C.: Residue burning in rice-wheat cropping system: Causes and
- 19 implications, *Curr. Sci.*, 87(12), 1713–1717, 2004.

- 20 Habib, G., Venkataraman, C., Chiapello, I., Ramachandran, S., Boucher, O. and Shekar Reddy,
- 21 M.: Seasonal and interannual variability in absorbing aerosols over India derived from TOMS:
- 22 Relationship to regional meteorology and emissions, *Atmos. Environ.*, 40(11), 1909–1921,
- 23 doi:10.1016/j.atmosenv.2005.07.077, 2006.

- 24 Huijnen, V., Wooster, M. J., Kaiser, J. W., Gaveau, D. L. A., Flemming, J. and Parrington, M.:
- 25 Fire carbon emissions over maritime southeast Asia in 2015 largest since 1997, *Nat. Publ. Gr.*,
- 26 (May), 1–8, doi:10.1038/srep26886, 2016.

- 27 Jaffe, L. S.: Ambient carbon monoxide and its fate in the atmosphere, *J. Air Pollut. Control*
- 28 *Assoc.*, 18(8), 534–540, doi:10.1080/00022470.1968.10469168, 1968.

- 29 Kaiser, J. W., Heil, A., Andreae, M. O., Benedetti, A., Chubarova, N., Jones, L., Morcrette, J.
- 30 J., Razinger, M., Schultz, M. G., Suttie, M. and van Der Werf, G. R.: Biomass burning
- 31 emissions estimated with a global fire assimilation system based on observed fire radiative
- 32 power, *Biogeosciences*, 9(1), 527–554, doi:10.5194/bg-9-527-2012, 2012.

- 33 Kariyathan, T., Pillai, D., Elias, E. and Mathew, T. A.: On deriving influences of upwind
- 34 agricultural and anthropogenic emissions on greenhouse gas concentrations and air quality over
- 35 Delhi in India: A Stochastic Lagrangian footprint approach, *Journal of Earth System Science*,
- 36 0123456789, doi:10.1007/s12040-020-01453-6, 2020.

- 37 Kretschmer, R., Gerbig, C., Karstens, U., Biavati, G., Vermeulen, A., Vogel, F., Hammer, S.



- 1 and Totsche, K. U.: Impact of optimized mixing heights on simulated regional atmospheric
2 transport of CO₂, Atmos. Chem. Phys. Discuss., 14(4), 4627–4685,
3 doi:10.5194/acpd-14-4627-2014, 2014.
- 4 Landgraf, J., Aan De Brugh, J., Scheepmaker, R., Borsdorff, T., Hu, H., Houweling, S., Butz,
5 A., Aben, I. and Hasekamp, O.: Carbon monoxide total column retrievals from TROPOMI
6 shortwave infrared measurements, Atmos. Meas. Tech., 9(10), 4955–4975, doi:10.5194/amt-9-
7 4955-2016, 2016.
- 8 Lasko, K. and Vadrevu, K.: Improved rice residue burning emissions estimates: Accounting for
9 practice-specific emission factors in air pollution assessments of Vietnam, Environ. Pollut.,
10 236, doi:10.1016/j.envpol.2018.01.098, 2018.
- 11 Mota, B. and Wooster, M. J.: Remote Sensing of Environment A new top-down approach for
12 directly estimating biomass burning emissions and fuel consumption rates and totals from
13 geostationary satellite fire radiative power (FRP), Remote Sens. Environ., 206(February
14 2017), 45–62, doi:10.1016/j.rse.2017.12.016, 2018.
- 15 NAAS: Innovative viable solution to rice residue burning in rice-wheat cropping system
16 through concurrent use of super straw management system-fitted combines and Turbo Happy
17 Seeder. Policy Brief No. 2. National Academy of Agricultural Sciences. New Delhi, India.
18 Available online at <http://naasindia.org/documents/CropBurning.pdf>, 2017.
- 19 Pillai, D., Buchwitz, M., Gerbig, C., Koch, T., Reuter, M., Bovensmann, H., Marshall, J. and
20 Burrows, J. P.: Tracking city CO₂ emissions from space using a high-resolution inverse
21 modelling approach: A case study for Berlin, Germany, Atmos. Chem. Phys., 16(15), 9591–
22 9610, doi:10.5194/acp-16-9591-2016, 2016.
- 23 Sahu, L. K., Sheel, V., Pandey, K., Yadav, R., Saxena, P. and Gunthe, S.: Regional biomass
24 burning trends in India: Analysis of satellite fire data, J. Earth Syst. Sci., 124(7), 1377–1387,
25 doi:10.1007/s12040-015-0616-3, 2015.
- 26 Schneising, O., Buchwitz, M., Reuter, M., Heymann, J., Bovensmann, H. and Burrows, J. P.:
27 Long-term analysis of carbon dioxide and methane column-averaged mole fractions retrieved
28 from SCIAMACHY, Atmos. Chem. Phys., 11(6), 2863–2880, doi:10.5194/acp-11-2863-2011,
29 2011.
- 30 Schneising, O., Burrows, J. P., Dickerson, R. R., Buchwitz, M. and Bovensmann, H.: Earth 's
31 Future Remote sensing of fugitive methane emissions from oil and gas production in North
32 American tight geologic formations, Earth ' s Future, 548–558, doi:10.1002/2014EF000265,
33 2014.
- 34 Schneising, O., Buchwitz, M., Reuter, M., Bovensmann, H., Burrows, J. P., Borsdorff, T.,
35 Deutscher, N. M., Feist, D. G., Griffith, D. W. T., Hase, F., Hermans, C., Iraci, L. T., Kivi, R.,
36 Landgraf, J., Morino, I., Notholt, J., Petri, C., Pollard, D. F., Roche, S., Shiomi, K., Strong, K.,
37 Sussmann, R., Velasco, V. A., Warneke, T. and Wunch, D.: A scientific algorithm to
38 simultaneously retrieve carbon monoxide and methane from TROPOMI onboard Sentinel-5
39 Precursor, Atmos. Meas. Tech., 12(12), 6771–6802, doi:10.5194/amt-12-6771-2019, 2019.



- 1 Schneising, O., Buchwitz, M., Reuter, M., Bovensmann, H. and Burrows, J. P.: Severe
- 2 Californian wildfires in November 2018 observed from space: The carbon monoxide
- 3 perspective, *Atmos. Chem. Phys.*, 20(6), 3317–3332, doi:10.5194/acp-20-3317-2020, 2020.
- 4 Sidhu, B., Rupela, O., Beri, V. and Joshi, P.: Sustainability Implications of Burning Rice-and
- 5 Wheat-Straw in Punjab, *Econ. Polit. Wkly.*, 33(39), 163A-168A, 1998.
- 6 Singh, C. P. and Panigrahy, S.: Characterisation of Residue Burning from Agricultural System
- 7 in India using Space Based Observations, *J. Indian Soc. Remote Sens.*, 39(3), 423–429,
- 8 doi:10.1007/s12524-011-0119-x, 2011.
- 9 Singh, T., Biswal, A., Mor, S., Ravindra, K., Singh, V. and Mor, S.: A high-resolution
- 10 emission inventory of air pollutants from primary crop residue burning over Northern India
- 11 based on VIIRS thermal anomalies, *Environ. Pollut.*, 266, 115132,
- 12 doi:10.1016/j.envpol.2020.115132, 2020.
- 13 Skamarock, W. C., Klemp, J. B., Dudhia, J. B., Gill, D. O., Barker, D. M., Duda, M. G.,
- 14 Huang, X.-Y., Wang, W. and Powers, J. G.: A description of the Advanced Research WRF
- 15 Version 3, NCAR Technical Note TN-475+STR, Tech. Rep., (June), 113,
- 16 doi:10.5065/D68S4MVH, 2008.
- 17 Steinbach, J., Gerbig, C., RÄdenbeck, C., Karstens, U., Minejima, C. and Mukai, H.: The CO₂
- 18 release and Oxygen uptake from Fossil Fuel Emission Estimate (COFFEE) dataset: Effects
- 19 from varying oxidative ratios, *Atmos. Chem. Phys.*, 11(14), 6855–6870, doi:10.5194/acp-11-
- 20 6855-2011, 2011.
- 21 Tai-Yi, Y.: Characterization of ambient air quality during a rice straw burning episode, *J.*
- 22 *Environ. Monit.*, 14(3), 817–829, doi:10.1039/c2em10653a, 2012.
- 23 Tripathi, S. N., Pattnaik, A. and Dey, S.: Aerosol indirect effect over Indo-Gangetic plain,
- 24 *Atmos. Environ.*, 41(33), 7037–7047, doi:10.1016/j.atmosenv.2007.05.007, 2007.
- 25 Venkataraman, C., Habib, G., Kadamba, D., Shrivastava, M., Leon, J.-F., Crouzille, B.,
- 26 Boucher, O. and Streets, D. G.: Emissions from open biomass burning in India: Integrating the
- 27 inventory approach with high-resolution Moderate Resolution Imaging Spectroradiometer
- 28 (MODIS) active-fire and land cover data, *Global Biogeochem. Cycles*, 20(2), n/a-n/a,
- 29 doi:10.1029/2005GB002547, 2006.
- 30 van der Werf, G. R., Randerson, J. T., Giglio, L., van Leeuwen, T. T., Chen, Y., Rogers, B. M.,
- 31 Mu, M., van Marle, M. J. E., Morton, D. C., Collatz, G. J., Yokelson, R. J. and Kasibhatla, P.
- 32 S.: Global fire emissions estimates during 1997–2016, *Earth Syst. Sci. Data*, 9(2), 697–720,
- 33 doi:10.5194/essd-9-697-2017, 2017.
- 34 Wang, T., Cheung, TF, Li, YS, Yu, XM, & Blake, DR. : Emission characteristics of CO, NO_x,
- 35 SO₂ and indications of biomass burning observed at a rural site in eastern China, *J. Geophys.*
- 36 *Res. Atmos.*, 107(D12), <http://dx.doi.org/10.1029/2001JD000724>, 2002
- 37 Ward, D. S., Kloster, S., Mahowald, N. M., Rogers, B. M., Randerson, J. T. and Hess, P. G.:



- 1 The changing radiative forcing of fires: Global model estimates for past, present and future,
- 2 *Atmos. Chem. Phys.*, 12(22), 10857–10886, doi:10.5194/acp-12-10857-2012, 2012.
- 3 Wunch, D., Toon, G. C., Blavier, J.-F. L., Washenfelder, R. A., Notholt, J., Connor, B. J.,
- 4 Griffith, D. W. T., Sherlock, V., and Wennberg, P. O.: The Total Carbon Column Observing
- 5 Network, *Philos. T. R. Soc. A*, 369, 2087–2112, <https://doi.org/10.1098/rsta.2010.0240>, 2011.
- 6 Yadav, S., Koli, P., Grassland, I. and Mina, U.: Popular Kheti, Popular Article, (January),
- 7 2018.
- 8 Zha, J., Li, B. Z., Shen, M. H., Hu, M. L., Song, H. and Yuan, Y. J.: Optimization of CDT-1
- 9 and XYL1 Expression for Balanced Co-Production of Ethanol and Xylitol from Cellobiose and
- 10 Xylose by Engineered *Saccharomyces cerevisiae*, *PLoS One*, 8(7), 1–8,
- 11 doi:10.1371/journal.pone.0068317, 2013.

12

13

14



1 Table 1. Overview of the TROPOMI CO products used in this study

Data ID	Satellite Data	Retrieval algorithm	Data access	Reference
WFMD	TROPOMI/WFMD CO	Weighting Function Modified Differential Optical Absorption Spectroscopy (WFM-DOAS)	(http://www.iup.uni-bremen.de/carbon_ghg/products/tropomi_wfmd/)	(Schneising et al., 2019, 2020)
SICOR	TROPOMI/SICOR CO	Shortwave Infrared Carbon Monoxide Retrieval (SICOR)	(https://scihub.copernicus.eu/)	(Landgraf et al., 2016; Borsdorff et al., 2018a, 2018b)

2

3



1 Table 2. List of ground-level measurement stations used for this study

No	Station name	State	Latitude (°N)	Longitude (°E)
1	Hardev Nagar, Bathinda - PPCB	Punjab	30.23	74.90
2	Civil Line, Jalandhar - PPCB	Punjab	31.32	75.57
3	Ratanpura, Rupnagar - Ambuja Cements	Punjab	30.00	76.60
4	NISE Gwal Pahari, Gurugram - IMD	Punjab	28.42	77.14
5	Burari Crossing, Delhi - IMD	Delhi	28.72	77.20
6	Delhi	Delhi	28.55	77.25
7	IGI Airport (T3), Delhi - IMD	Delhi	28.56	77.11
8	ITO, Delhi - CPCB	Delhi	28.62	77.24
9	Lodhi Road, Delhi - IMD	Delhi	28.59	77.22
10	NSIT Dwarka, Delhi - CPCB	Delhi	28.60	77.03



11	Patparganj, Delhi - DPCC	Delhi	28.62	77.28
12	Sector - 125, Noida - UPPCB	Utter Pradesh	28.50	77.30
13	Sanjay Palace, Agra - UPPCB	Utter Pradesh	27.20	78.00
14	Central School, Lucknow - CPCB	Utter Pradesh	26.88	80.93
15	Ardhali Bazar, Varanasi - UPPCB	Utter Pradesh	25.40	82.90
16	IGSC Planetarium Complex, Patna - BSPCB	Bihar	25.60	85.10
17	Ghusuri, Howrah - WBPCB	West Bengal	22.61	88.34
18	Padmapukur, Howrah - WBPCB	West Bengal	22.56	88.27
19	Rabindra Bharati University, Kolkata - WBPCB	West Bengal	22.62	88.38
20	Victoria, Kolkata - WBPCB	West Bengal	22.54	88.34



1 Table 3. Comparison between WFMD and SICOR products over India during the burning
2 period and the full month of November 2018. Abbreviations N, MB, SD, and R correspond to
3 the number of observations, mean bias, standard deviation of differences, and correlation
4 coefficient respectively.

5

Peak Burning Period Only (6-9 November 2018)	N (SICOR): 93416 N (WFMD): 98093 MB (SICOR-WFMD): 1.85 ppb SD (SICOR-WFMD): 4.86 ppb R (SICOR vs. WFMD): 0.97
All of November 2018	N (SICOR): 555724 N (WFMD): 638215 MB (SICOR-WFMD): 1.72 ppb SD (SICOR-WFMD): 4.27 ppb R (SICOR vs. WFMD): 0.97

6

7

8

9

10

11



- 1 Table 4. Contribution from different emissions sources to the CO concentration at ground level
2 (GL) between 6-9 and 3-20 November 2018. Abbreviations ANT, BBU and BCK represent
3 anthropogenic, biomass burning, and background signals respectively (see Sect. 3)

4

Period	CO	Delhi			Punjab			IGP		
		ANT	BBU	BCK	ANT	BBU	BCK	ANT	BBU	BCK
6 – 9 November 2018	Column	35 %	12 %	53 %	21 %	14 %	65 %	32 %	5 %	63 %
	Surface	83 %	10 %	7 %	49 %	38 %	13 %	79 %	10 %	11 %
3 – 20 November 2018	Column	43 %	6 %	51 %	25 %	8 %	67 %	34 %	3 %	63 %
	Surface	86 %	4 %	10 %	60 %	17%	23 %	82 %	4 %	14 %

5

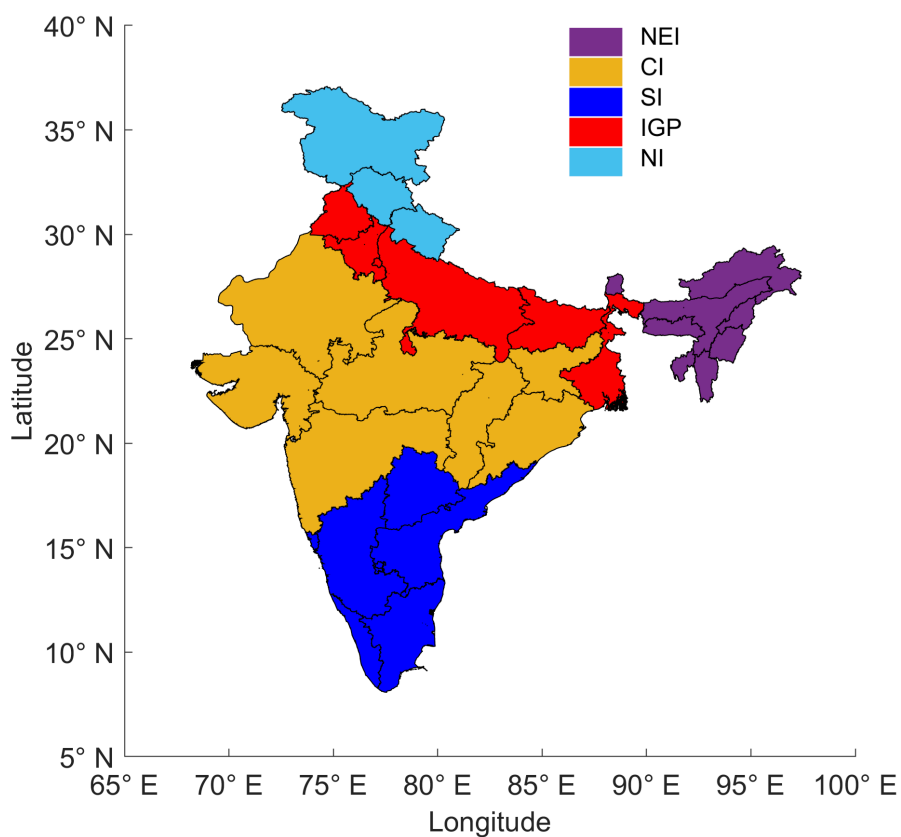
6

7

8

9

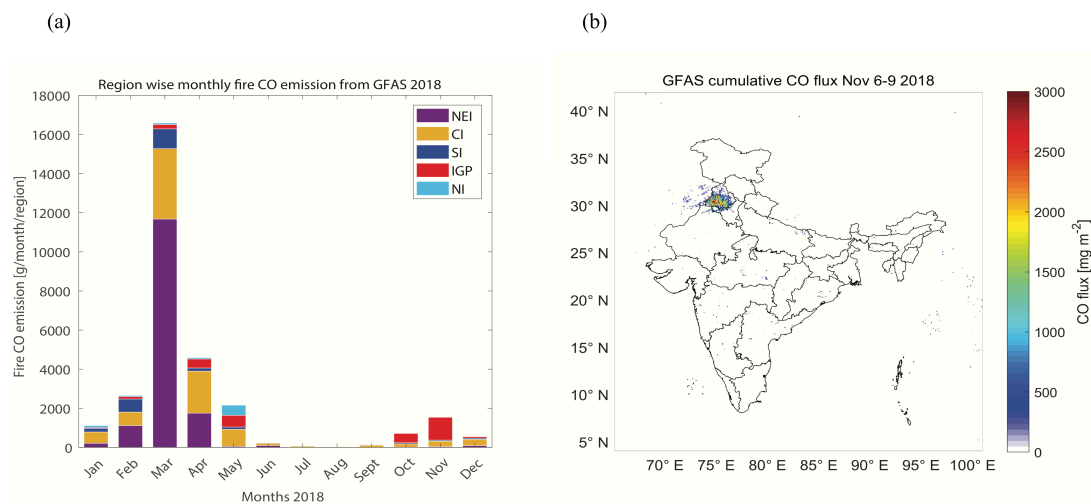
10



1

2 **Figure 1** India partitioned into five different areas for analysis: northeast India (NEI), central
3 India (CI), southern India (SI), the Indo-Gangetic Plain (IGP), and northern India (NI).

4



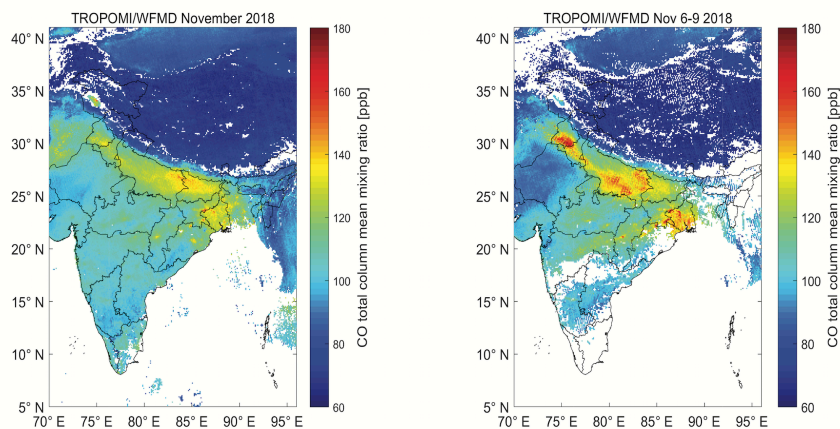
1

2 **Figure 2 (a)** The monthly integrated GFAS fire CO emissions ($\text{mg}/\text{m}^2/\text{month}$) over different
3 regions of India (as seen in Figure 1) during the year 2018. **(b)** Integrated GFAS fire CO
4 emission during 6-9 November 2018.

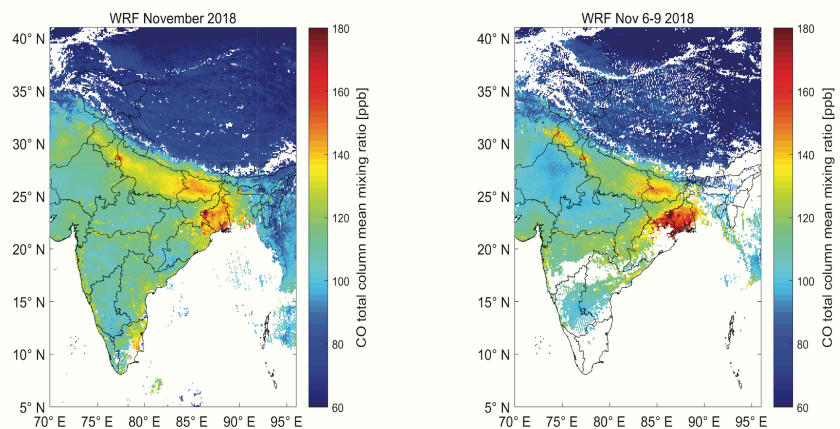
5



(a) TROPOMI/WFMD

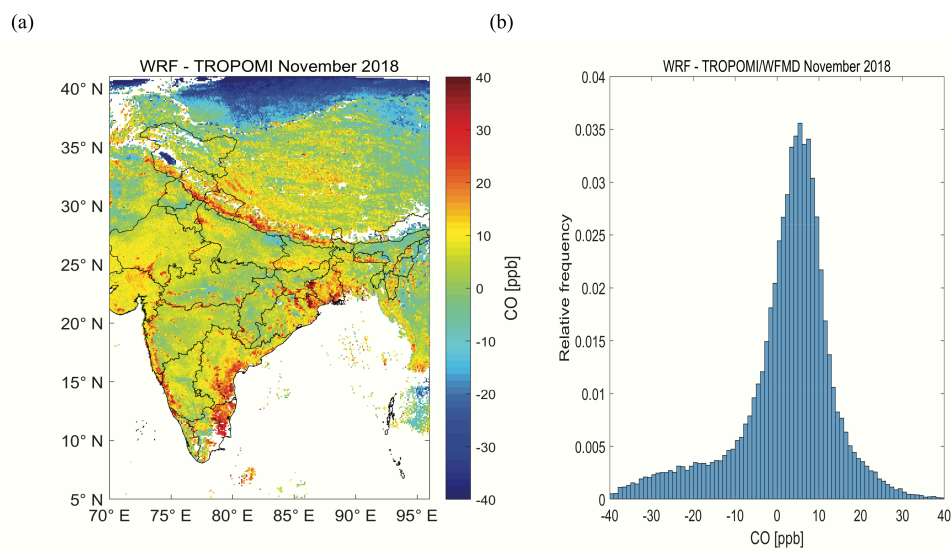


(b) WRF



1
2
3
4
5

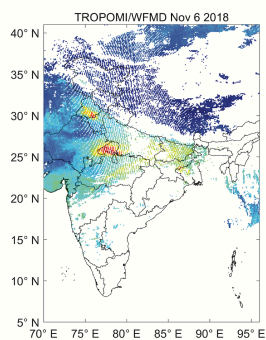
Figure 3: CO total column mixing ratios averaged over all of November 2018 (left panel) and from 6-9 November 2018 (right panel). **(a)** TROPOMI/WFMD **(b)** WRF model



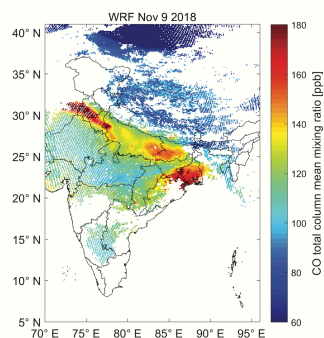
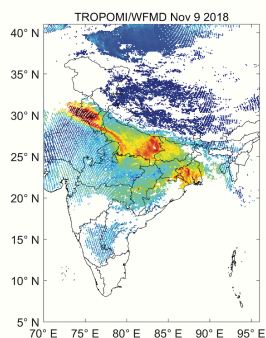
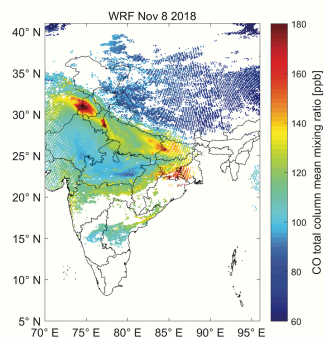
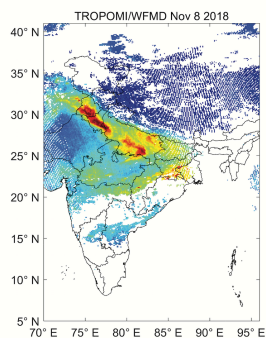
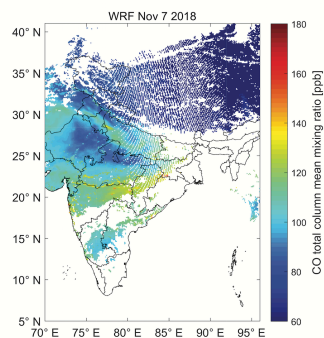
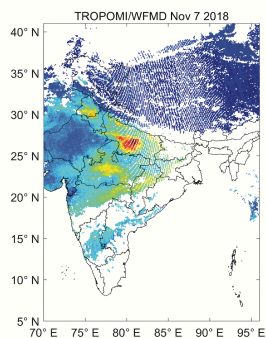
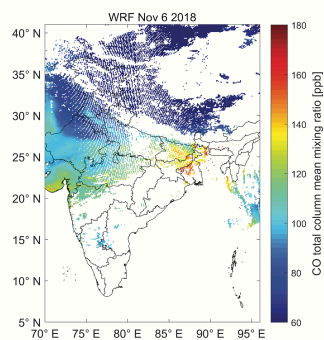
1
2 **Figure 4:** (a) Differences of CO total column mixing ratios (WRF –TROPOMI/WFMD)
3 averaged over the month of November 2018. (b) Histogram of the differences (Mean bias: 7
4 ppb; standard deviation: 8 ppb; correlation coefficient: 0.87).
5



(a)

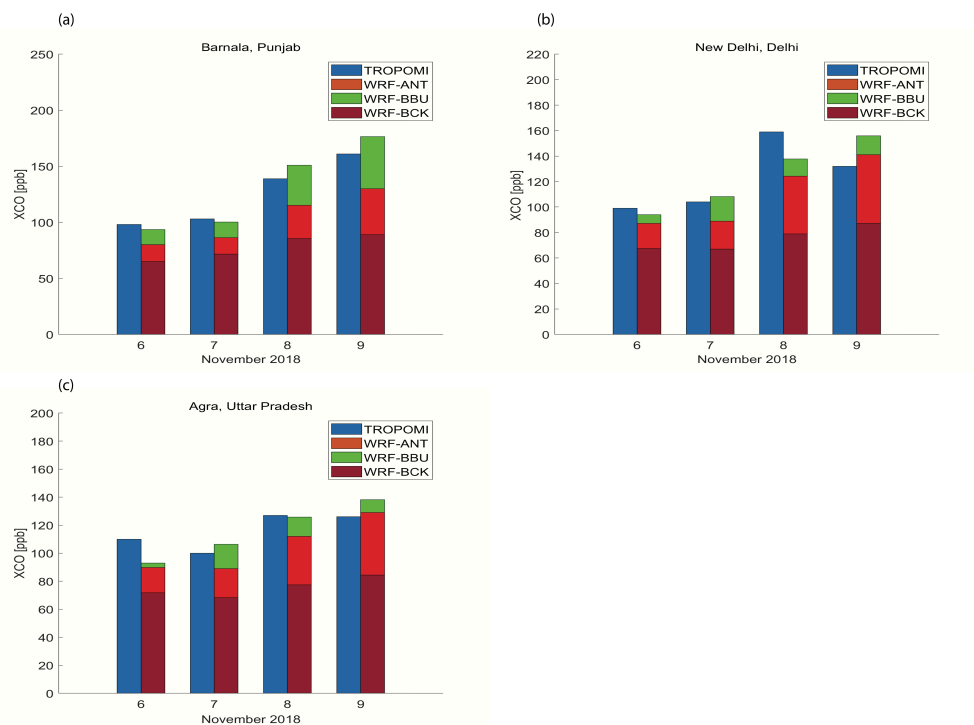


(b)



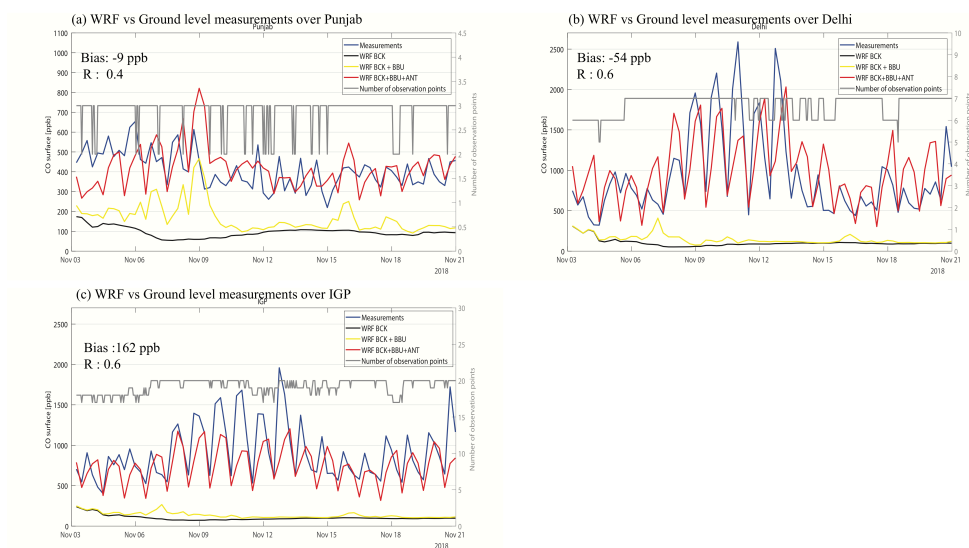


- 1 **Figure 5:** (a) Daily column CO observations from TROPOMI/WFMD (left panels) and (b)
- 2 collocated WRF simulation (right panels) for November 6-9 2018.
- 3



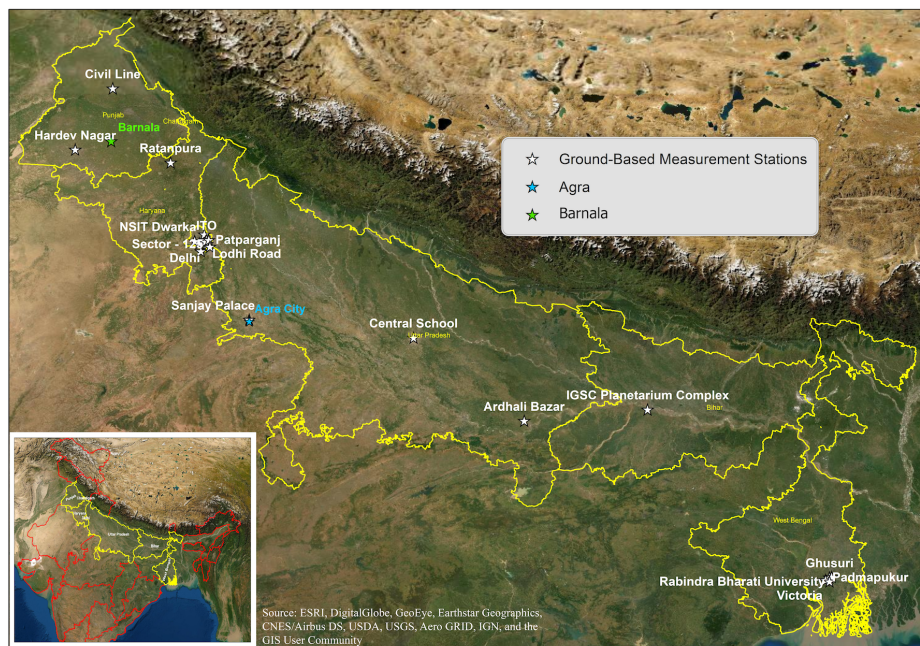
1
2 **Figure 6:** Carbon monoxide (CO) total column mixing ratios over (a) Barnala, (b) New Delhi,
3 and (c) Agra for individual days from 6–9 November 2018.

4



1
2
3
4

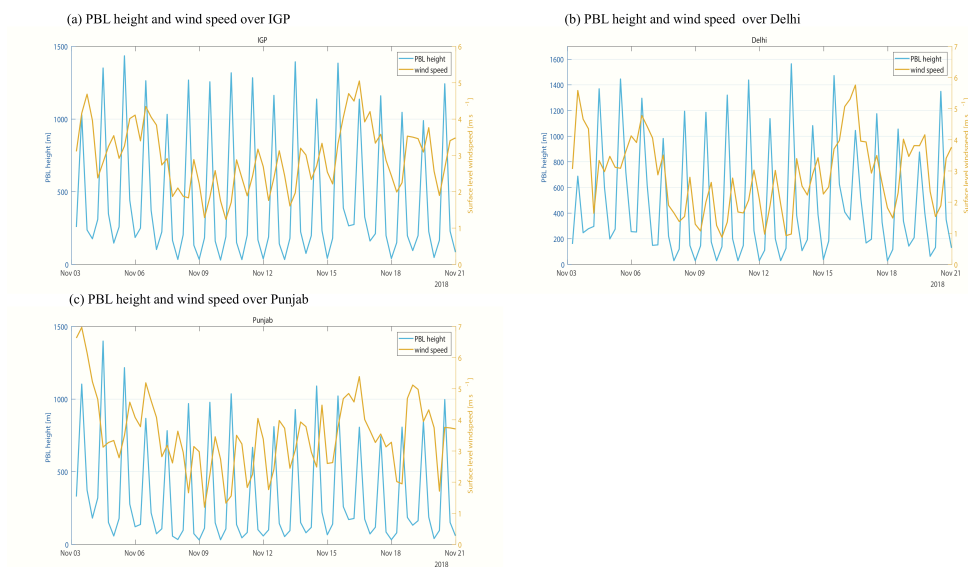
Figure 7: Ground level CO measurements and WRF model simulations for a period of 3-20 November 2018 over (a) the IGP region (b) Delhi (c) Punjab.



1

2 **Figure 8:** Map showing the locations of sites used for model evaluation. The yellow contour
3 represents the IGP region. The inset image shows the broader region for context.

4



1

2 **Figure 9:** PBL height and surface level wind speed from WRF model simulations for a period
3 of 3-20 November 2018 over (a) the IGP region, (b) Delhi, and (c) Punjab.

4

5

6

7

8

9

10